Received: 24 February 2025 | Accepted: 16 August 2025

DOI: 10.1002/fob2.70024

RESEARCH ARTICLE

FOOD BIOMACROMOLECULES

WILEY

Carrageenan hard capsules reinforced with cellulose nanocrystals dissolved in deep eutectic solvent and hydroxypropyl methylcellulose

Chigozie Charity Okwuwa[1] | Fatmawati Adam[1,2] | Michael E. Ries[3] | Farhan Mohd Said[1] | Samuel Olugbenga Olunusi[1]

[1]Faculty of Chemical and Process Engineering Technology, Universiti Malaysia Pahang Al-Sultan Abdullah, Lebuh Persiaran Tun Khalil Yaakob, Kuantan, Pahang, Malaysia

[2]Centre for Research in Advanced Fluid and Processes, Universiti Malaysia Pahang, Al-Sultan Abdullah, Kuantan, Pahang, Malaysia

[3]School of Physics and Astronomy, University of Leeds, Leeds, UK

Correspondence
Fatmawati Adam.
Email: fatmawati@umpsa.edu.my

Funding information
UMPSA, Grant/Award Numbers: PGRS230302, RDU223012

Abstract

Carrageenan-based biocomposites are promising materials due to their biodegradability, cost-effectiveness and wide availability, making them suitable for food and drug delivery applications. This study addresses the brittle nature of refined carrageenan by reinforcing it with cellulose nanocrystal (CNC) dissolved in choline chloride lactic acid-based deep eutectic solvent (DES) and comparing the mechanical performance of formulations with and without hydroxypropyl methylcellulose (HPMC). Four formulations were developed: 3WH (3-g carrageenan with HPMC), 3WOH (3 g without HPMC), 5WH (5 g with HPMC) and 5WOH (5 g without HPMC). The 5WH formulation demonstrated superior mechanical properties, including a tensile strength of 89.37 MPa, a capsule loop strength of 49.33 MPa and a viscosity of 1217.00 $mPas^{-1}$, which indicated excellent mechanical performance and structural integrity. Molecular modelling using Gaussian software was conducted to investigate the interactions between CNC and DES, revealing an interaction energy of 1995 kJ/mol and an enthalpy of formation of −3123.75 kJ/mol. The bond distance between DES components was observed as 2.48 and 1.98 Å, with angles changing from 23.5° to 128° upon dissolution. The disappearance of peaks in the ^{1}H nuclear magnetic resonance spectra evidenced this. These findings offer valuable insights into the molecular interactions in cellulose dissolution and pave the way for innovative plant-based hard capsules for industrial applications.

KEYWORDS
carrageenan, cellulose dissolution, deep eutectic solvent, hydrogen bonding, molecular structure

1 | INTRODUCTION

Sustainability has become a crucial focus in materials science and engineering due to growing environmental concerns and the depletion of nonrenewable resources. One emerging field within this domain is the development of biocomposite materials made from natural polymers reinforced with fibres or fillers.[1,2] These biocomposites offer several advantages, such as biodegradability, renewable sourcing and reduced environmental impact. Among the various biopolymers available, carrageenan, a polysaccharide derived from red seaweed, has gained attention due to its wide availability, biocompatibility and versatile properties.[3,4] Carrageenan is extensively used in the food, pharmaceutical and cosmetics industries, primarily due to its ability to form gels, bind water and stabilise emulsions.[5] However, carrageenan-based materials often exhibit poor mechanical strength and thermal stability despite these favourable properties, thus limiting their industrial applications.[6] Addressing these limitations is essential for expanding the use of carrageenan-based biocomposites, particularly in high-performance applications such as hard capsules for the pharmaceutical industry.[7]

One promising approach to improve the properties of carrageenan biocomposites is through the reinforcement of cellulose nanocrystals (CNCs) dissolved in deep eutectic solvent (DES) and the inclusion of hydroxypropyl methylcellulose (HPMC). HPMC, a semi-synthetic polymer derived from cellulose, is widely recognised for its excellent film-forming ability, biocompatibility and mechanical reinforcement properties. It has been used in pharmaceutical and food applications as a stabiliser, binder and thickening agent.[8,9] When combined with carrageenan, HPMC acts as a co-binder, thereby improving the mechanical strength, flexibility and water resistance of biocomposites.[10]

CNC is derived from cellulose, the most abundant natural biopolymer, and possesses exceptional mechanical properties, including high tensile strength, stiffness and a high aspect ratio.[11] These properties make CNC ideal for reinforcing polymer matrices and enhancing their mechanical and thermal behaviour.[12] However, incorporating CNC into biopolymer matrices such as carrageenan presents significant challenges.[13] CNCs are insoluble in water and most organic solvents due to the strong hydrogen bonds in the crystalline regions of cellulose.[14,15] This leads to poor dispersion of CNCs within the polymer matrix, resulting in suboptimal reinforcement and reduced performance of the biocomposite.[16] Therefore, developing efficient and environmentally friendly methods for dissolving CNCs is critical for their successful integration into carrageenan-based biocomposites. DESs have emerged as a promising class of green solvents for dissolving and processing cellulose.[17] They are formed by mixing two or more components, typically a hydrogen bond donor (HBD) and a hydrogen bond acceptor (HBA), which together form a eutectic mixture with a melting point lower than that of the individual components.[18] DESs have gained considerable attention because they are biodegradable, less toxic and more cost-effective than conventional solvents, making them suitable for large-scale industrial applications. Choline chloride (ChCl), a common HBA in DES formulations, is known for its low toxicity and biodegradability, making it an ideal component for green solvent systems, and lactic acid, which occurs naturally as an organic acid, serves as the HBD.[19] The combination of chloride and lactic acid forms a DES that can break the strong hydrogen bonds in the crystalline regions of cellulose, facilitating the dissolution of CNCs.[20] This DES system offers a novel solution for improving the dispersion and interfacial adhesion of CNCs in carrageenan matrices, thereby enhancing the mechanical reinforcement of the biocomposite.[21,22]

Computational modelling using Gaussian 09W simulation has provided insights into the interaction mechanism between CNCs and DES.[23] From the study of Ramli et al., the simulation results showed the formation of a hydrogen bond between the oxygen atom of cellulose and the chlorine atom of ChCl, with a bond length of approximately 1.57 Å.[24] This bond length falls within the range of strong hydrogen bonding, which is typically electrostatic and has bond energies between 4 and 15 kcal/mol.[25] This moderate hydrogen bonding is essential for maintaining the structural integrity of CNCs while allowing for sufficient dissolution and dispersion within the biopolymer matrix.[26] Additionally, the improved solubility and dispersion of CNCs in DES play a critical role in enhancing the mechanical and thermal behaviour of the resulting biocomposite,[21,22] exhibiting higher tensile strength and thermal stability compared to unreinforced carrageenan films.[28] Carrageenan-reinforced biocomposites achieved tensile strengths exceeding 100 MPa and melting temperatures above 240°C, indicating their suitability for high-performance applications, including hard capsule production for the pharmaceutical industry.[29] This study aims to enhance the carrageenan biocomposite by incorporating CNCs dissolved in a ChCl-lactic acid-based DES into the carrageenan matrix. Four distinct biocomposite formulations were systematically analysed to identify the one offering the most favourable mechanical and physical properties.

2 | EXPERIMENTAL SECTION

2.1 | Materials

The refined carrageenan (molecular weight ranges from 930 to 1010 $nmol^{-1}$) with 31.5% carbon, 5.97% hydrogen, 0% nitrogen and 6.28% sulphur was acquired from CV Simpul Agro Globalindo, Indonesia.[3,4] 4-Methoxybenzyl alcohol (98%) (anise), calcium alginic acid (alg) and HPMC (1261.4 g/mol) were purchased from Sigma-Aldrich. PEG was purchased from Merck (Germany) as a plasticiser. The constituents of chloride (98%, 139.62 g/mol), lactic acid (99.5%, 90.08 g/mol) and microcrystalline cellulose (MCC) (Avicel PH-101) were also purchased from Sigma-Aldrich. A Milli-Q water system was used to prepare deionised water, and all chemicals used were analytical.

2.2 | Preparation of DES, CNC and carrageenan biocomposite films

2.2.1 | Preparation of DES

ChCl underwent pretreatment to remove any moisture by being heated in a vacuum oven overnight at 80°C before being used.[21,22] Dried ChCl with lactic acid at a molar ratio of 1:1 was continuously stirred for 3 h at 200 rpm under a temperature of 60°C to obtain a homogeneous mixture with no evidence of solid particles. The eutectic mixture formed was kept as the DES.

2.2.2 | Preparation of CNC and dissolution in DES

CNC dissolution in DES was conducted using a method reported by Zhang et al. with modification. 0.2 g of MCC was gradually added to 10 g of DES in a flask under continuous stirring for 12 h. This was ultrasonicated at a frequency of 20 kHz and a power of 100 W for 30 min to achieve cellulose nanocrystal in deep eutectic solvent (CNCDES). 5 mL of CNCDES was separated by centrifugation at 5000 rpm for 3 min and washed with deionised water to get the regenerated CNC.[31] This was used for further characterisation.

2.2.3 | Dissolution of CNC in DES used for formulation

To achieve CNCDES, 0.2 g of MCC was added to 10 g of DES solution and continuously stirred for 12 h. 10 mL of DI water was also added and continuously stirred. Only 2 mL of the solution was used in each sample formulation.[32,33]

2.2.4 | Preparation of carrageenan biocomposite films and hard capsule

The method used by Ramli et al.[21,22] was adopted with modifications in this study; four formulations for carra-CNCDES-HPMC and carra-CNCDES biocomposite films were prepared. Two formulations used 3.0 g of refined carrageenan (3WH and 3WOH), and the other two used 5.0 g of refined carrageenan (5WH and 5WOH), each mixed with 2.0 w/v% HPMC. The 3.0-g carrageenan was prepared in 60 mL of deionised water, and the 5.0-g carrageenan was prepared in 100 mL at 60°C with stirring. Each sample received 2.0 v/v% CNCDES, 0.5 v/v% anise, 1.5 v/v% PEG and 0.2 w/v% calcium alginate as a cross linker, plasticiser and toughening agent, respectively. After 5 h of mixing, 20 mL of each solution was poured into a 20-cm diameter stainless steel tray and left overnight to form films. Rigid capsules were created by casting the remaining solution using stainless-steel mould capsule pins. The dried films and hard capsules were then characterised and analysed.[34]

2.3 | Testing and characterisation

2.3.1 | Gaussian 09W analysis

The B3LYP (Becke's three-parameter functional and nonlocal correlation of LYP expression) level of theory was used to perform the density functional theory (DFT) calculations using Gaussian 09W software with a basis set of 6-31G (d, p). The optimisation of geometry and frequency computations for ChCl and lactic acid, which were used to prepare DES, was executed with the selected functional and correlation functions.[35] DES and cellulose chemical structures were also optimised to determine the interaction between DES and cellulose. The geometry-optimised calculation generated the molecular electronic surface potential (MESP) and interaction energy of ChCl, lactic acid, the combined structure of ChCl and lactic acid (DES), and cellulose in the DES. Conjugate complexes with Mulliken charge were drawn through the MESP evaluation.[36] The interaction points and hydrogen bond lengths between the molecular structures were measured for each conjugate complex. The quantum mechanics evaluation was used to calculate the hydrogen bond interaction energy and enthalpy formation using Equations (1) and (2), respectively.

$$\text{Interaction energy} = \text{ESCF complex} - (\text{ESCF DES} + \text{ESCF CNC}) \quad (1)$$

$$\Delta H\text{formation} = H\text{complex} - (H\text{DES} + H\text{CNC}) \quad (2)$$

ESCF is the energy of the self-consistent field generated from the optimisation calculation, whereas H is the sum of the electronic and thermal enthalpies generated by the frequency calculation.

2.3.2 | ^{1}H NMR analysis

The nuclear magnetic resonance (NMR) investigation was carried out by identifying the preferred intermolecular interactions to gain molecular-level understanding through changes in DES's proton (^{1}H) spectrum. A ^{1}H NMR spectrometer, Bruker UltraShield Plus, operating at room temperature, was used to record the 500-MHz ^{1}H NMR spectra. Samples in deuterated dimethyl sulphoxide (DMSO-d6) were used as the internal standard.[37] The chemical shifts were calculated by DMSO-d6's retained proton resonance (2.50 ppm).[38]

2.3.3 | Fourier transform infrared analysis

The identification of various functional groups present in DES and the four formulations of carrageenan biocomposite films was conducted through Fourier transform infrared spectroscopy (FTIR) to observe potential shifts in chemical bonds during the formation of DES. The samples were analysed using a FTIR spectrometer (PerkinElmer Frontier) equipped with OMNIC software. At a resolution of 4 cm^{-1}, the spectra were obtained between 4000 and 400 cm^{-1}.[21,22]

2.3.4 | X-ray diffraction analysis

The samples' X-ray diffractograms were acquired using a Siemens D5000 diffractometer utilising Cu-Kα radiation (λ = 15.4 nm, 40 kV and 30 mA) at a temperature of 25°C. The relative intensity was documented within a scattering angle range (2θ) of 5°–40°. The crystalline peaks were first detected to acquire the results on crystallinity.[39] Crystalline peaks that corresponded to cellulose ≠β were (056) at 10.84 2θ, (096) at 13.24 2θ, (134) at 16.44 2θ, (254) at 21 2θ and (258) at 22.7 2θ. The Gaussian function was employed as the curve-fitting function in Origin 2018 software, which was used to separate crystalline and amorphous contributions for crystallinity computation. Consequently, the ratio of the area of each crystalline peak to the overall area was used to compute crystallinity.[40]

2.3.5 | Viscosity analysis

The viscosity of a biocomposite plays a critical role in determining its mechanical properties, as it reflects the strength of intermolecular interactions within the carrageenan matrix. Higher viscosity signifies stronger bonding between molecules, contributing to enhanced material strength. The viscosity and shear stress of the biocomposite solution were assessed using a rotational viscometer (Brookfield Rheo3000) equipped with an LCT 25 4000010 geometry. Approximately 16.5 mL of the biocomposite solution was loaded into the cylindrical measurement chamber for each measurement. The analysis was conducted in triplicate at a constant temperature of 40°C, using a rotational speed of 300 rpm and 100 Mpoints, and the results were presented as mean values ± standard deviation (SD).[41]

2.3.6 | Morphological analysis by scanning electron microscopy

A scanning electron microscope, GeminiSEM 300, running at a 5-kV accelerating voltage, analysed the morphology of the samples. To avoid electrical charging effects, the samples were coated with platinum for 300 s at 40 mA using a sputter coater BalTec/Leica SCD050 before being examined under a scanning electron microscope. They were secured onto stubs using carbon tabs.

2.3.7 | Mechanical tests

The mechanical evaluation assessed the deformation characteristics of the films and hard capsules under applied load. A texture analyser (CT3) with TexturePro CT V1-8 Build 3.1 software and a 5-kN load cell measured the biocomposite film's tensile strength and elongation at break (EAB). Tensile strength measurements followed ASTM D882-12 standards. Films were cut into 20 mm × 100 mm strips, and thickness was averaged from three measurements using Vernier callipers. The texture analyser settings included an 80-mm initial grip separation (gauge length), a crosshead speed of 30 mm/min and a maximum displacement of 15 mm. For each formulation, tensile strength and EAB were measured in triplicate. The values of load at break and elongation at rupture were recorded directly from the texture analyser, and tensile strength and EAB were subsequently calculated using standard formulas, and results were reported as mean ± SD.

$$\text{Tensile Strength (MPa)} = \frac{\text{Load at break}}{\text{Initial width} \times \text{Initial thickness}} \quad (3)$$

$$\text{Elongation at break (\%)} = \frac{\text{Enlogation at rupture}}{\text{Initial guage length}} \times 100\% \quad (4)$$

The same texture analyser (CT3) was used to conduct the capsule loop test but with a capsule loop fixture. A hard capsule was attached to a pair of separating rods, with the lower rod positioned on the stationary platform and centrally beneath the probe. The upper rod gradually went higher at a speed of 0.50 mm/s with a target value of 5.0 mm until the hard capsule was torn apart.[42] The applied force (*N*) to break the hard capsule was reported as the capsule loop strength. The analysis was conducted with three measurements for each sample to calculate the average result.

2.3.8 | Moisture content

Moisture content (MC) can influence the mechanical and thermal stability of hard capsules. Therefore, a moisture analyser was utilised to determine the capsule MC. The initial weight of the capsules, as well as the final mass after the heating process at 40°C was completed, was compared to their original mass to calculate the MC.[43] The measurement concluded once the samples' MC stabilised at a constant value; this analysis was conducted in triplicate at a constant temperature.

2.3.9 | Water vapour permeability

The water vapour permeability (WVP) of the film samples was determined by ASTM E-96 (1990), with modifications as described by Maryam Adilah et al.[44] Initially, a crucible was filled with 6 mL of distilled water, and the film was positioned over the opening of the crucible to ensure complete coverage. Vacuum grease was applied to create a tight seal. The samples prepared were then placed in a desiccator maintained at 50% ± 5% relative humidity and 23°C ± 2°C. The analysis was conducted in triplicate, and the weight of the samples was recorded hourly until a constant weight was achieved, typically around 9 h. The WVP ($gm^{-1}\ s^{-1}\ Pa^{-1}$) was subsequently calculated using Equation (5).

$$\text{WVP} = \frac{\text{weight difference}}{(\text{Exposed area}) \times (\text{Time}) \times (\text{Pressure difference})} \quad (5)$$

3 | RESULTS AND DISCUSSION

3.1 | Computational modelling of DES: Molecular interactions and thermodynamics insight

Predictive techniques grounded in the electronic configuration of reactants have been used in this study, covering a range of techniques, such as measurable analyses of molecular surfaces to ascertain electrostatic potential. This analytical approach is important, both theoretically and practically, in recognising the reactive site at the molecular surface.[45] The optimised MESP illustrated the charge distribution between CNC and the DES, as shown in Figure 1. It equally illustrated the electrostatic potential profiles of key components, including ChCl, lactic acid and their 1:1 DES combination, and composite systems such as cellobiose and DES amalgamations. Mulliken charge analysis has been instrumental in characterising these profiles, revealing intriguing details about the charge distribution within the molecules. Figure 1a exhibits the MESP charge of choline chloride, showing the distribution of electrostatic charges on the molecule. A highly negative region (region I, MC: −0.094) is observed around the chloride ion (8Cl), appearing as a red patch, which signifies its electron-rich nature and strong potential as an HBA. Additionally, a positive potential region (region II, MC: 0.061) is localised around the hydroxyl proton (22H on the 7O atom), identified by a blue hue, indicating its suitability as an HBD. This electrostatic distribution reflects the amphiphilic behaviour of ChCl, with distinct donor and acceptor sites, enabling it to participate effectively in noncovalent interactions typical in DES formation.[37] Figure 1b presents the electrostatic potential map of lactic acid, revealing its hydrogen bonding capabilities through differential charge distribution. Region III (MC: −0.043) is located near the carboxylic acid group, particularly around the carbonyl oxygen (10O), and is characterised by a red area denoting an electron-rich HBA zone. Meanwhile, region IV (MC: 0.066) appears around the hydroxyl proton (12H on 20O), represented in blue, signifying an HBD region due to its positive electrostatic potential. This spatial distribution of potential across the lactic acid molecule underscores its bifunctional role in hydrogen bonding, capable of both donating and accepting protons, which is essential in stabilising interactions with HBAs like ChCl in DES systems.[36] Figure 1c displays the molecular interaction between ChCl and lactic acid in the DES system, highlighting the synergistic hydrogen bonding that stabilises the DES structure. The chloride ion (region V, MC: −0.075) remains the most negative site, reaffirming its role as a strong HBA. Region VI (MC: 0.075), a positive potential region, surrounds the hydroxyl hydrogen (22H on 7O), acting as an HBD. Notably, two significant hydrogen bonds are observed: one between the chloride ion and 16H (2.48 Å) and another between the chloride and 34H (1.98 Å), with an interaction angle of 23.5°, all of which confirm stable and directional bonding. This interaction map validates the formation of a robust DES through electrostatic complementarity and hydrogen bonding between ChCl and lactic acid, critical for its physicochemical properties and potential applications. Figure 1d highlights distinct electron-rich and electron-deficient regions, indicating potential sites for intermolecular interactions. Region VII, with a moderately negative molecular charge (MC: −0.043), is indicative of electron-rich zones such as oxygen atoms that could act as HBAs. In contrast, region VIII exhibits a slightly positive charge (MC: 0.068), suggesting a proton-donating site likely involved in hydrogen bonding. The red dashed circles emphasise hydroxyl groups contributing to these electrostatic regions. These zones play a crucial role in the interaction potential of cellobiose with other polar molecules, particularly through hydrogen bonding, which is vital for its dissolution and compatibility with green solvents such as DES.[25,46] Figure 1e illustrates the interaction between cellobiose and the DES, showing a pronounced hydrogen bond network. Region IX (MC: −0.064) and region X (MC: 0.045) denote zones of electron richness and deficiency, respectively, facilitating strong hydrogen bonding. Notably, a hydrogen bond is observed between the hydroxyl groups of cellobiose and the functional moieties of DES, with a bond distance of 2.48 Å and an angle of 128°, signifying stable and directional bonding.[47] The interaction leads to a spatial alignment between DES and cellobiose, evidenced by a dihedral angle of 51.48° and a proximity of 3.24 Å between critical atoms.[48] This confirms effective DES-cellobiose complex formation, which enhances the solubility and structural compatibility of cellulose in the green solvent system. The observed bond distances between the DES were 2.48 Å and 1.98 Å at the angle of 23.5°, and the angle increased to 128° after dissolution occurred, coupled with an interaction energy of 1995 KJ/mol and an enthalpy formation of Δ3123.75 KJ/mol, which underscores the strength and stability of hydrogen bond interactions in DES systems.

3.2 | Effects of CNC in choline chloride lactic acid DES on ^{1}H NMR spectra

The NMR spectra in Figure 2a,b provide detailed insights into the chemical environment of the DES system composed of ChCl and lactic acid (1:1-M ratio) and its interaction with CNCs. Figure 2a represents the spectrum of the DES alone. The peaks in the DES spectrum, as shown in Table 1, are labelled from P1 to P7, representing different proton environments. P1 is observed at 1.26, 1.25, 1.29, 1.30, 1.40 and 1.42 ppm, corresponding to the methyl groups of ChCl, which remain relatively unchanged upon CNC dissolution.[49] However, minor shifts are observed at 1.24, 1.25, 1.29, 1.30, 1.40 and 1.42 ppm in Figure 2b. P2 appears at 2.54 and 2.55 ppm in the DES spectrum but is absent in the CNCDES system, suggesting an interaction between CNC and the DES that has led to a change in the local electronic environment of protons responsible for these peaks. P3, representing protons at 3.05, 3.20, 3.48, 3.49 and 3.50 ppm, undergoes noticeable shifts upon CNC addition, with new peaks at 3.17, 3.21, 3.25, 3.50, 3.51 and 3.52 ppm, indicating interactions between CNC hydroxyl groups and the DES components.[50] Similarly, P4, originally at 3.83, 3.84 and 3.85 ppm, remains mostly unchanged except for a minor retention of the 3.84 ppm peak in the CNCDES system. This demonstrates that these protons may not be

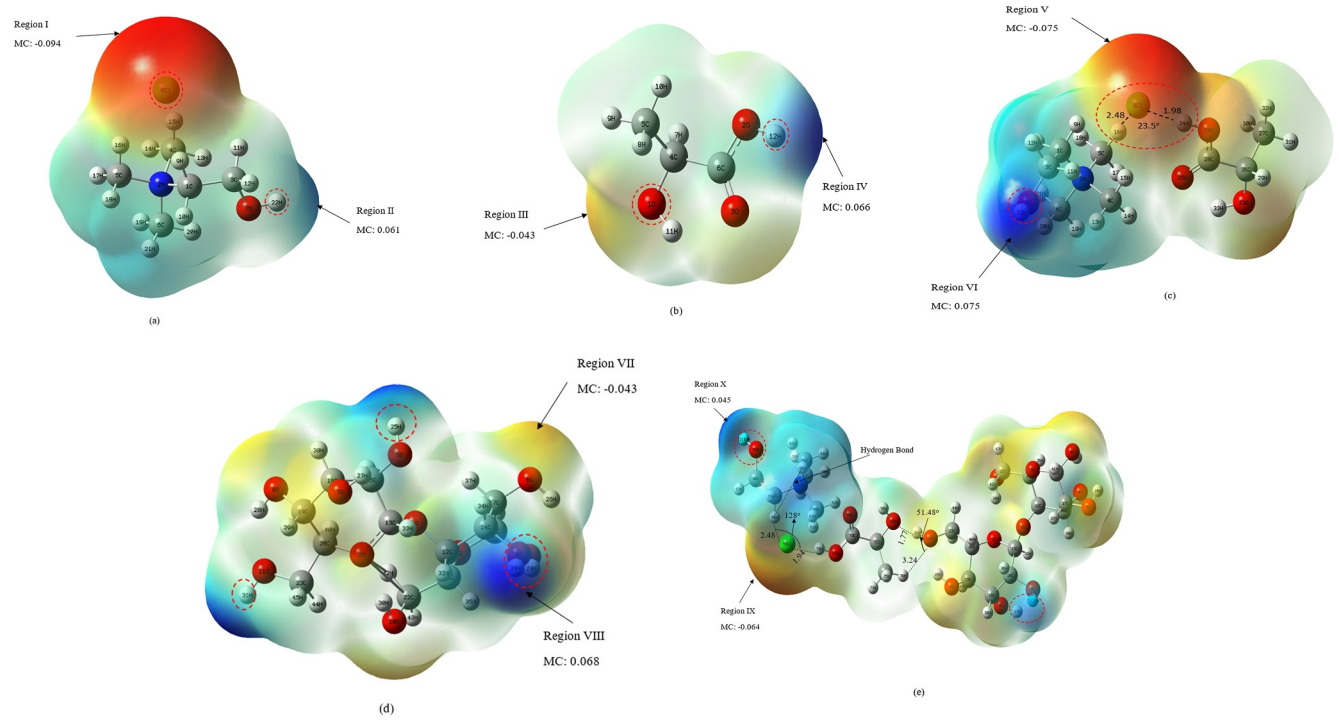

FIGURE 1 3D plots of molecular electrostatic surface potential. (a) Electrostatic surface potential of choline chloride, (b) lactic acid, (c) DES, (d) cellulose, (e) cellulose in DES. DES, deep eutectic solvent.

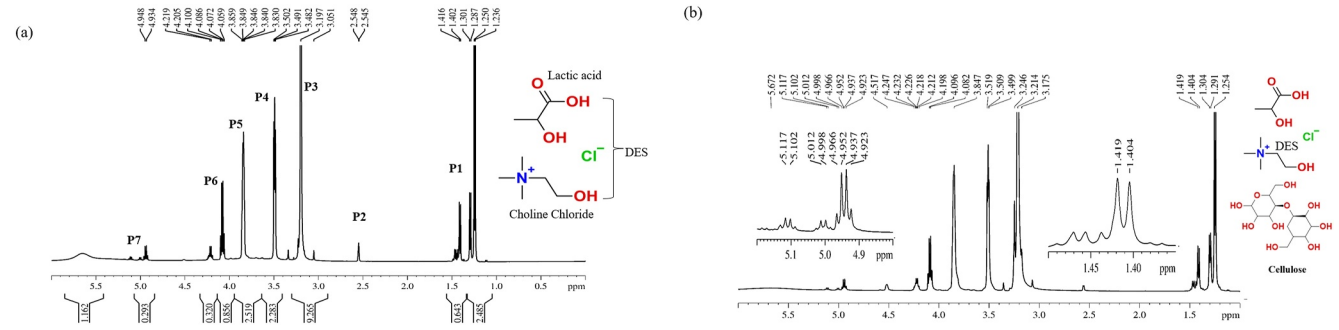

FIGURE 2 (a) Complex ^{1}H nuclear magnetic resonance spectra. (a) Choline chloride lactic acid-DES (1:1). (b) Cellulose nanocrystal dissolved in choline chloride lactic acid-DES (1:1). DES, deep eutectic solvent.

TABLE 1 Different peaks of DES and CNC dissolved in DES.

	DES peaks (ChCl and lactic acid) (1:1)	CNC in DES peaks
P1	1.26, 1.25, 1.29, 1.30, 1.40, 1.42	1.24, 1.25, 1.29, 1.30, 1.40, 1.42
P2	2.54, 2.55	-
P3	3.05, 3.20, 3.48, 3.49, 3.50	3.17, 3.21, 3.25, 3.50, 3.51, 3.52
AP4	3.83, 3.84, 3.85	3.84
P5	4.06, 4.07, 4.09, 4.10	4.08, 4.10
P6	4.20, 4.22	4.21, 4.22, 4.23, 4.25, 4.52, 4.92, 4.94, 4.95, 4.97, 4.99
P7	4.93, 4.94	5.01, 5.10, 5.12, 5.67

Abbreviations: CNC, cellulose nanocrystal; DES, deep eutectic solvent.

significantly influenced by CNC addition. The P5 peaks at 4.06, 4.07, 4.09 and 4.10 ppm exhibit minor changes, shifting slightly to 4.08 and 4.10 ppm in the CNCDES system, further supporting molecular interactions between CNC hydroxyl groups and the DES matrix. P6, which appears at 4.20 and 4.22 ppm in the DES spectrum, broadens significantly upon CNC addition, with new peaks at 4.21, 4.22, 4.23, 4.25, 4.52, 4.92, 4.94, 4.95, 4.97 and 4.99 ppm, suggesting an extensive involvement of CNC in modifying the hydrogen bonding network of DES.[38] The most significant change is observed in P7, initially at 4.93 and 4.94 ppm, which shifted in the CNCDES spectrum to 5.01, 5.10, 5.12 and 5.67 ppm, indicative of CNC hydroxyl functionalities strongly engaging in the hydrogen bonding with the DES components.[45] The additional peaks in the higher chemical shift region (4.9–5.1 ppm) in the CNCDES spectrum suggest the presence of hydrogen-bonded protons between CNC and the DES matrix, which further confirms the successful dissolution of CNC within the DES system. This is also supported by the MESP interaction. Hydrogen bonding plays a major role in stabilising CNC within the DES environment.

3.3 | Characterisation of CNC, DES, CNC in DES and CNCDES-carra biocomposite film

CNC dissolved in ChCl lactic acid-based DES at 1:1, as shown in the FTIR plot in Figure 3a, presents special peaks of CNC at 3885.83, 3281.72, 2237.52 and 1654.15 cm^{-1}, corresponding to the stretching vibrations of saturated C–H, O–H, unsaturated C≡C and C=O bonds. DES peaks were found at 3303.00, 2984.34 and 1724.24 cm^{-1},[51] indicating the stretching vibrations of O–H, unsaturated C=O and saturated N–H bonds, respectively.[52] Only the individual cellulose peak was discernible in the finished film, whereas the specific peaks of CNC dissolved in DES vanished. This demonstrates that the CNC dissolved in DES was eliminated from the sample's surface, which proves that a significant amount of CNC was dissolved in DES after the peak disappeared and later appeared only at 2983.79 and 1725.06 cm^{-1}, in contrast to the CNC peaks alone.[53] The C-OH and unsaturated C=O are represented as the 2983.79 and 1725.06 cm^{-1} peaks in the CNC dissolved in the DES spectrum. The peaks of CNC dissolved in DES were easily visible in the samples before regeneration, suggesting that DES and CNC were properly integrated, as supported by the findings of FTIR. Figure 3b shows the CNC curve characteristic diffraction peaks at 2θ values of 15.9°, 16.2° and 22.54°, which are typical of cellulose I structure, indicating its semicrystalline nature. After dissolution in DES, as shown in the CNCDES curve, the intensity of the main peak at 22.54° significantly increases and a new peak appears at 34.6°. This suggests that a modification in the crystalline structure and enhanced crystallinity, as well as a molecular reorganisation due to interactions between the CNC and the DES components, occurred.[54] DES oxygen atoms created hydrogen bonds with cellulose, aiding its breakdown.[47] The analysis of the CNCDES-carra biocomposite film using FTIR provided insights into the molecular composition and interactions within the material. In Figure 3c,d, specific peaks observed confirmed the presence of various components and their bonding characteristics. The cellulose component exhibited a distinctive peak at 1054 cm^{-1}, attributed to the C-O-C bonding within the cellulose structure. Upon incorporating carrageenan into the biocomposite film at different weight ratios, new peaks emerged, indicating changes in the molecular environment. For instance, in the 3WH sample, peaks were detected at 2919.38, 1243.11 and 731.11 cm^{-1}, corresponding to C≡C, C-C and C-Cl bonds, respectively.[55] These characteristics bore a resemblance to polycarbonic acid and ethyl vinyl acetate. Similarly, the 3WOH biocomposite film exhibited peaks at 3366.30, 1740.39, 1637.11 and 1157.71 cm^{-1}, corresponding to O-H, C-O, C=C and C-O bonds.[51] These features were reminiscent of compounds such as 3,4-dimethylbenzyl alcohol and 1,6-heptadien-4-ol. In the case of the 5WH sample, peaks were detected at 1245.83, 1063.40 and 731.53 cm^{-1}, corresponding to C-O, C-C and C-Cl bonds, resembling compounds such as 2-fluoroethanol and glycerol. Meanwhile, the 5WOH sample exhibited peaks at 1064.01 and 731.53 cm^{-1}, corresponding to C-C bonds,[56] indicating similarities to certain compounds. These observations suggest that the dissolution of cellulose in DES for the formulation of carrageenan biocomposite films resulted in interactions between cellulose molecules. These interactions likely led to the breakdown of hydrogen bonds present in cellulose,[57] as evidenced by the changes in peak characteristics observed in the FTIR analysis. Figure 3d presents the X-ray diffraction analysis patterns of CNCDES-carra biocomposite films with and without HPMC at different weights of carrageenan (3 and 5 g). The diffraction peaks observed around 10°, 21° and 31° indicate semicrystalline behaviour typical of polysaccharide materials. Among the samples, those containing HPMC (3WH and 5WH) exhibit sharper and more intense peaks, particularly at 21° compared to their HPMC-free counterparts (3WOH and 5WOH). This suggests that the incorporation of HPMC enhances the overall crystallinity of the biocomposites.

3.4 | Mechanical properties of CNC in DES and CNCDES-carra biocomposite film

In evaluating the properties of carrageenan-based biocomposites with and without the addition of HPMC, significant differences emerged in terms of WVP, tensile strength, elongation at break, crystallinity, capsule loop strength, viscosity and tensile stress. Specifically, 3WH refers to 3 g of carrageenan with HPMC, 3WOH refers to 3 g of carrageenan without HPMC, 5WH refers to 5 g of carrageenan with HPMC, and 5WOH refers to 5 g of carrageenan without HPMC. These formulations illustrate how both the amount of carrageenan and the presence of HPMC can affect the material's overall performance, particularly in applications related to pharmaceutical capsules and packaging.

WVP is a critical factor in determining the effectiveness of a biocomposite as a moisture barrier. The data reveal that WH samples (those containing HPMC) consistently show higher WVP values than WOH samples. 3WH exhibits a WVP of

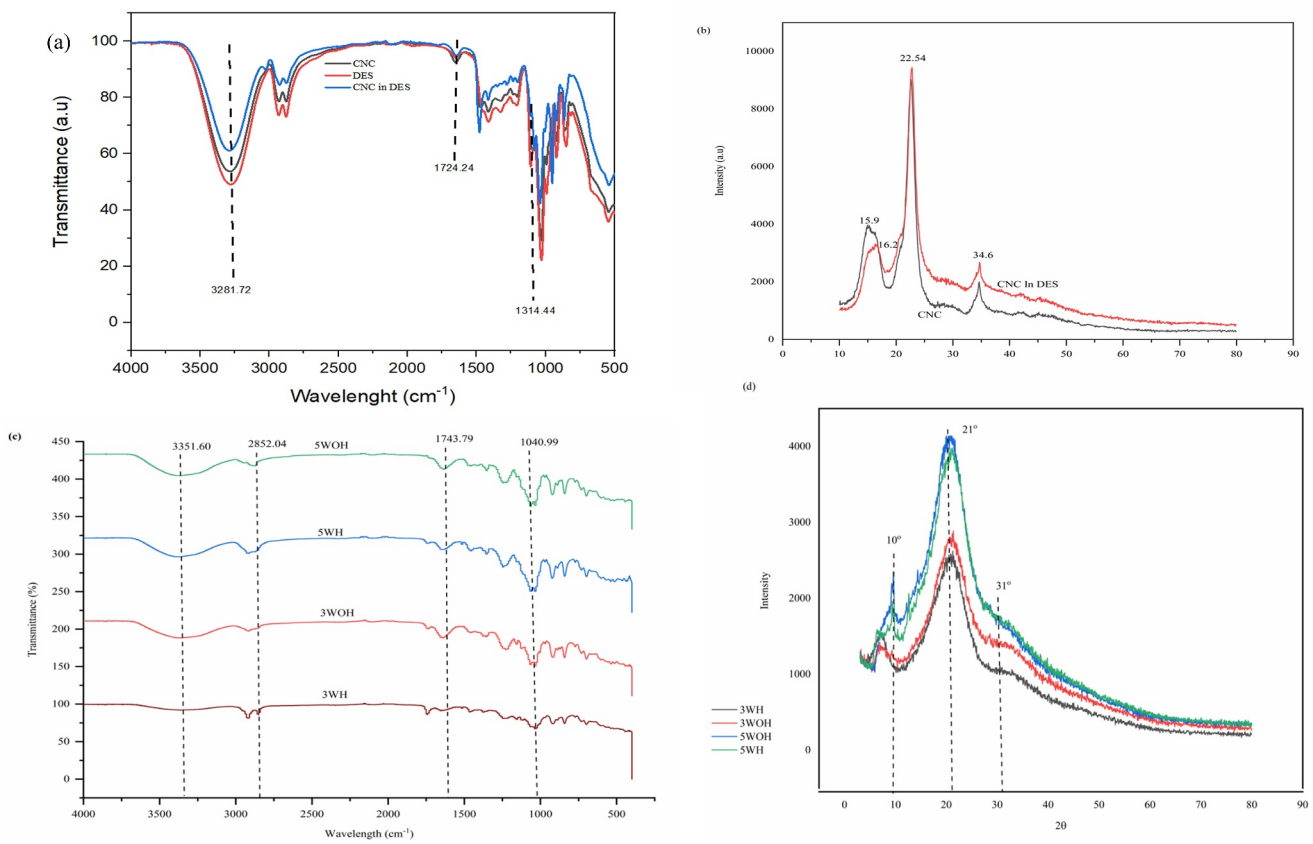

FIGURE 3 Characterisation of CNCDES-carrageenan film. (a) FTIR of CNC, DES and CNC dissolved in DES (b), XRD of CNC, DES and CNC dissolved in DES (c), FTIR spectra of CNCDES-carra film (d), XRD of CNCDES-carra biocomposite of different weights. CNC, cellulose nanocrystal; CNCDES, cellulose nanocrystal in deep eutectic solvent; DES, deep eutectic solvent; FTIR, Fourier transform infrared spectroscopy; XRD, X-ray diffraction analysis.

3.37×10^{-12} g·m^{-1}·s^{-1}·Pa^{-1}, which is significantly higher than the 1.44×10^{-12} g·m^{-1}·s^{-1}·Pa^{-1} observed for 3WOH. Similarly, 5WH has a WVP of 3.16×10^{-12} g·m^{-1}·s^{-1}·Pa^{-1}, whereas 5WOH shows a lower WVP of 1.50×10^{-12} g·m^{-1}·s^{-1}·Pa^{-1}. This suggests that the inclusion of HPMC increases the permeability of the carrageenan matrix to water vapour, likely due to the hydrophilic nature of HPMC.[58] HPMC is known for its water-attracting properties, which could contribute to increased molecular mobility within the biocomposite, thereby facilitating water vapour diffusion. In contrast, samples without HPMC (WOH) exhibit lower WVP values, indicating that the absence of this hydrophilic agent results in a denser, less permeable structure. Because of their lower permeability to water vapour, the WOH formulations may be more suitable for applications where moisture barrier properties are critical, such as in food or pharmaceutical packaging. This finding aligns with previous research by Sanyang et al.,[59] who observed that the water content and the type of polymer additives used in biocomposites can significantly impact their barrier properties, with hydrophilic additives generally increasing WVP.

Tensile strength, a measure of the material's resistance to breaking under tension, also shows clear differences between the WH and WOH samples and between the different carrageenan concentrations, as shown in Figure 4. The tensile strength of 5WH, which contains 5 g of carrageenan with HPMC, is remarkably high at 89.00 MPa compared to 36.67 MPa for 5WOH. This difference suggests that combining a higher carrageenan content with HPMC significantly enhances the material's tensile strength, likely due to improved interactions between the carrageenan matrix and the HPMC. Similarly, the tensile strength of 3WH is 43.67 MPa, almost double that of 3WOH (21.33 MPa), as illustrated in Figure 4a, reinforcing the idea that HPMC plays a critical role in improving the mechanical properties of the biocomposite. HPMC enhanced the dispersion of carrageenan and provided additional hydrogen bonding sites, improving the material's cohesion and load-bearing capacity.[60] Researchers found similar results in their study of polysaccharide-based films, where the addition of reinforcing agents such as HPMC improved tensile strength by promoting better interactions between polymer chains. Elongation at break, which measures how much the material can stretch before breaking, shows less dramatic but still noticeable differences between the WH and WOH samples. The values for elongation at break remain relatively similar across all samples, ranging from 35% to 38%. For instance, 3WH shows an elongation at break of 36.51%, whereas 3WOH has a similar value of 36.35%. In the case of the 5-g samples, 5WH has an elongation at

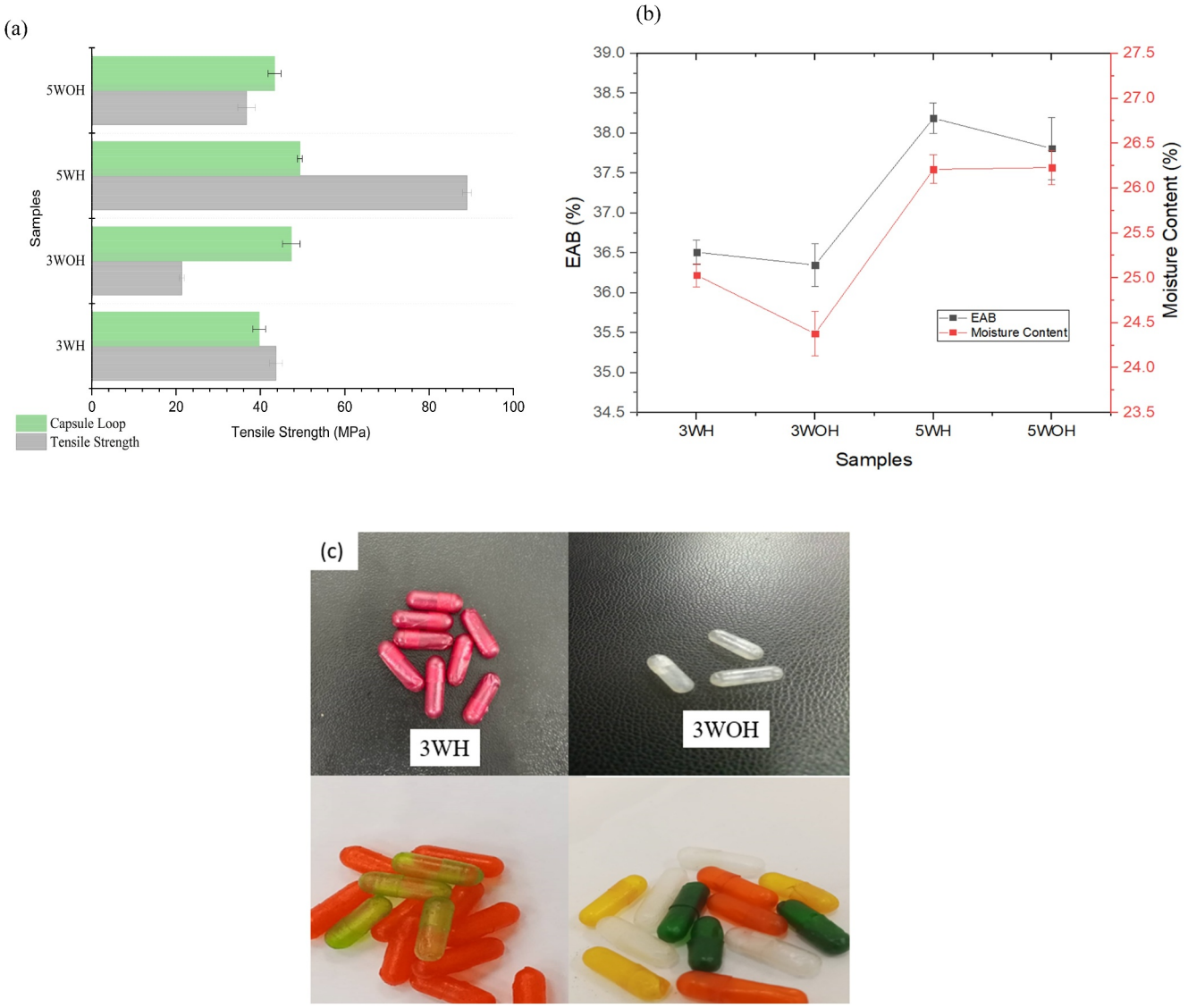

FIGURE 4 The biocomposite films' mechanical properties. (a) Tensile/capsule loop strength versus CNCDES-carra concentration in weight. (b) Elongation at break/moisture content of the varied weight of carrageenan. (c) Pictorial view of the different types of CNCDES-carra hard capsules. CNCDES, cellulose nanocrystal in deep eutectic solvent.

break of 38.19%, whereas 5WOH closely follows with 37.81%. These results suggest that although the presence of HPMC may slightly improve the flexibility of the biocomposite, the overall impact on elongation is minimal. This may be because carrageenan already possesses moderate flexibility, and the addition of HPMC does not significantly alter its elongation ability. However, the slight increase in elongation at break observed in WH samples could be attributed to the plasticising effect of HPMC, which may soften the material slightly and allow for more stretch before breaking. This property is particularly important in pharmaceutical applications, where capsules need some flexibility to withstand mechanical stress during handling and ingestion without breaking prematurely.

Crystallinity, as seen in Table 2, is a measure of the degree of structural order in the material, showing a significant variation between WH and WOH samples. The inclusion of HPMC appears to increase crystallinity in both the 3- and 5-g samples. For instance, 3WH has a crystallinity of 65.20% compared to 52.10% for 3WOH, whereas 5WH exhibits a crystallinity of 83.60% compared to 78.80% for 5WOH. The higher crystallinity in WH samples indicates that the addition of HPMC promotes the formation of more ordered crystalline structures within the carrageenan matrix due to the ability of HPMC to facilitate better alignment and packing of polymer chains. Higher crystallinity is associated with improved mechanical strength, as the crystalline regions in the material provide greater resistance to deformation under stress. This explains why the WH samples exhibit higher tensile strength compared to their WOH counterparts. The findings are consistent with Wan Ishak et al.,[61] who reported that the addition of reinforcing agents can enhance the crystallinity of polysaccharide-based films, leading to improved mechanical properties. Capsule loop strength, which is a measure of the mechanical

TABLE 2 Mechanical properties, elongation and crystallinity of films using different weights of carrageenan.

Carra-hard capsules	Viscosity ($mPas^{-1}$)	Tensile strength (MPa)	Capsule loop strength (MPa)	WVP ($\times 10^{-12}$ $g{\cdot}m^{-1}{\cdot}s^{-1}{\cdot}Pa^{-1}$)	Moisture content (%)	Elongation at break (%)	Crystallinity (%)
3WH	770.00 ± 5.51	43.67 ± 1.53	39.67 ± 1.53	3.37 ± 3.01	25.03 ± 0.13	36.51 ± 0.15	65.20
3WOH	605.00 ± 4.51	21.33 ± 0.58	47.30 ± 2.08	1.44 ± 0.24	24.38 ± 0.25	36.35 ± 0.27	52.10
5WH	1217.00 ± 2.52	89.00 ± 1.00	49.33 ± 0.58	3.16 ± 0.52	26.21 ± 0.16	38.19 ± 0.19	83.60
5WOH	897.00 ± 2.52	36.67 ± 2.08	43.33 ± 1.53	1.50 ± 0.55	26.23 ± 0.19	37.81 ± 0.39	78.80

integrity of capsules formed from these biocomposites, is another critical parameter for pharmaceutical applications. The capsule loop strength, as shown in the WH samples, is higher than that of the WOH samples, particularly in the 5-g formulations. 5WH has a capsule loop strength of 49.18 MPa compared to 43.30 MPa for 5WOH. Additionally, 3WH has a capsule loop strength of 39.30 MPa compared to 47.20 MPa for 3WOH. This trend suggests that the presence of HPMC improves the mechanical integrity of the capsules, making them more resistant to mechanical stress.[24] The improved capsule loop strength in WH samples could be due to the enhanced interaction between HPMC and the carrageenan matrix, leading to a more cohesive and mechanically robust structure. This is particularly important in pharmaceutical applications, where capsules must maintain their integrity during handling, storage and ingestion. The higher capsule loop strength of WH samples makes them more suitable for applications where mechanical performance is critical.

Viscosity, which measures the material resistance to flow, is significantly higher in WH samples compared to WOH samples. For instance, 5WH has a viscosity of 1217.00 $mPas^{-1}$ compared to 897.00 $mPas^{-1}$ for 5WOH, whereas 3WH has a viscosity of 770.00 $mPas^{-1}$ compared to 605.00 $mPas^{-1}$ for 3WOH. The higher viscosity in WH samples can be attributed to the presence of HPMC, which increases the overall molecular interactions within the biocomposite, resulting in higher resistance to flow. HPMC is known for its thickening properties, which could explain the significant increase in viscosity observed in WH samples. Higher viscosity may be advantageous in certain processing applications,[62] such as extrusion or casting, where greater control over the material's flow properties is required. The increased viscosity of WH samples also suggests that they will be easier to mould and shape into capsules or other forms during manufacturing. Adding HPMC to carrageenan biocomposites significantly enhances their mechanical and thermal properties, including tensile strength, crystallinity and capsule loop strength, while increasing WVP and viscosity.[63] These improvements make WH samples more suitable for applications requiring high mechanical performance, such as pharmaceutical capsules, although the increased WVP may limit their use in moisture-sensitive applications. Figure 4b illustrates the EAB and MC of the film samples (3WH, 3WOH, 5WH and 5WOH), each presented with mean values and SD from repeated measurements ($n = 3$). A *t*-test was conducted to evaluate the statistical significance of differences between the samples. The results showed that both EAB and MC increased significantly ($p < 0.05$) with the addition of HPMC and higher carrageenan concentration, particularly in the 5WH sample, indicating enhanced film flexibility and water retention. The significant differences among the formulations confirm that both HPMC incorporation and carrageenan content play critical roles in determining the mechanical and moisture properties of the films. Figure 4c presents the visual appearance of hard capsules formulated with varying carrageenan concentrations (3 and 5 g) and the presence or absence of HPMC. Capsules containing HPMC (3WH and 5WH) exhibit vibrant and uniform colours, indicating improved pigment entrapment, film formation and overall aesthetic quality. In contrast, the capsules without HPMC (3WOH and 5WOH) appear translucent or inconsistently coloured, suggesting weaker structural integrity and less effective pigment distribution. The combination of higher carrageenan content and HPMC (5WH) results in the most visually appealing capsules, highlighting the synergistic effect of both components in enhancing capsule quality.

4 | CONCLUSION

The utilisation of Gaussian simulation to explore the interaction between cellulose and ChCl lactic acid-based DES has shown that cellulose hydrogen bonds can be broken down. These findings, corroborated by FTIR analysis and validated by DFT calculations and ^{1}H NMR spectra, underscore the pronounced intermolecular hydrogen bonding between CNC and DES. The robust interaction has remarkably reinforced the mechanical integrity of both carrageenan biocomposite films and hard capsules. Additionally, the observed dissolution rate that CNCDES enhanced in the structural and mechanical properties upon decomposition was evidenced by the disappearance of major peaks from the ^{1}H NMR spectra after the dissolution of CNC in DES occurred. However, there remains a need to explore the CNCDES and carrageenan matrix. Future research should optimise the CNCDES formulation, evaluate long-term stability and assess the biodegradability and nontoxicity of the developed biocomposites for broader industrial applications.

AUTHOR CONTRIBUTIONS

Chigozie Charity Okwuwa: Experimental and theoretical methodology; visualization; conceptualization; data curation and analysis; writing—original draft. **Fatmawati Adam**: Supervision; writing;

review and editing. **Michael E. Ries**: Writing—review and editing; validation. **Farhan Mohd Said**: Writing—review and editing. **Samuel Olugbenga Olunusi**: Writing—review and editing.

ACKNOWLEDGEMENTS

The authors express their gratitude to Universiti Malaysia Pahang Al-Sultan Abdullah for providing research funding through the UMPSA Internal Grant RDU223012 and PGRS230302.

CONFLICT OF INTEREST STATEMENT

The authors declare no conflicts of interest.

DATA AVAILABILITY STATEMENT

The datasets used and analysed during this study are available from the corresponding author upon reasonable request.

ETHICS STATEMENT

Not applicable.

CONSENT

Not applicable.

ORCID

Chigozie Charity Okwuwa https://orcid.org/0009-0000-6264-8695
Fatmawati Adam https://orcid.org/0000-0001-8748-2812
Michael E. Ries https://orcid.org/0000-0002-8050-3200
Farhan Mohd Said https://orcid.org/0000-0003-0737-3486
Samuel Olugbenga Olunusi https://orcid.org/0009-0008-5039-6329

REFERENCES

1. Andrew, J. J., and H. N. Dhakal. 2022. "Sustainable Biobased Composites for Advanced Applications: Recent Trends and Future Opportunities – A Critical Review." *Composites Part C: Open Access* 7: 100220. https://doi.org/10.1016/j.jcomc.2021.100220.
2. Hultman, L., S. Mazur, C. Ankarcrona, A. Palmqvist, M. Abrahamsson, M.-L. Antti, M. Baltzar, et al. 2024. "Advanced Materials Provide Solutions Towards a Sustainable World." *Nature Materials* 23(2): 160–1. https://doi.org/10.1038/s41563-023-01778-9.
3. Adam, F., J. Jamaludin, S. H. Abu Bakar, R. Abdul Rasid, and Z. Hassan. 2020. "Evaluation of Hard Capsule Application From Seaweed: Gum Arabic-Kappa Carrageenan Biocomposite Films." *Cogent Engineering* 7(1): 1765682. https://doi.org/10.1080/23311916.2020.1765682.
4. Adam, F., J. Jamaludin, S. H. Abu Bakar, R. Abdul Rasid, and Z. Hassan. 2020. "Evaluation of Hard Capsule Application From Seaweed: Gum Arabic-Kappa Carrageenan Biocomposite Films." *Cogent Engineering* 7(1): 1765682. https://doi.org/10.1080/23311916.2020.1765682.
5. Udo, T., G. Mummaleti, A. Mohan, R. K. Singh, and F. Kong. 2023. "Current and Emerging Applications of Carrageenan in the Food Industry." *Food Research International* 173: 113369. https://doi.org/10.1016/j.foodres.2023.113369.
6. Asadzadeh, N., M. Ghorbanpour, and A. Sayyah. 2023. "Effects of Filler Type and Content on Mechanical, Thermal, and Physical Properties of Carrageenan Biocomposite Films." *International Journal of Biological Macromolecules* 253: 127551. https://doi.org/10.1016/j.ijbiomac.2023.127551.
7. Aga, M. B., A. H. Dar, G. A. Nayik, P. S. Panesar, F. Allai, S. A. Khan, R. Shams, J. F. Kennedy, and A. Altaf. 2021. "Recent Insights Into Carrageenan-Based Bio-Nanocomposite Polymers in Food Applications: A Review." *International Journal of Biological Macromolecules* 192: 197–209. https://doi.org/10.1016/j.ijbiomac.2021.09.212.
8. Al-Tabakha, M. M. 2010. "HPMC Capsules: Current Status and Future Prospects." *Journal of Pharmacy & Pharmaceutical Sciences* 13(3): 428. https://doi.org/10.18433/J3K881.
9. Majee, S. B., D. Avlani, and G. R. Biswas. 2017. "HPMC as Capsule Shell Material: Physicochemical, Pharmaceutical and Biopharmaceutical Properties." *International Journal of Pharmacy and Pharmaceutical Sciences* 9(10): 1. https://doi.org/10.22159/ijpps.2017v9i10.20707.
10. Ku, M. S., Q. Lu, W. Li, and Y. Chen. 2011. "Performance Qualification of a New Hypromellose Capsule: Part II. Disintegration and Dissolution Comparison Between Two Types of Hypromellose Capsules." *International Journal of Pharmaceutics* 416(1): 16–24. https://doi.org/10.1016/j.ijpharm.2011.02.048.
11. Grishkewich, N., N. Mohammed, J. Tang, and K. C. Tam. 2017. "Recent Advances in the Application of Cellulose Nanocrystals." *Current Opinion in Colloid & Interface Science* 29: 32–45. https://doi.org/10.1016/j.cocis.2017.01.005.
12. Danial, W. H., R. M. Taib, M. A. A. Samah, and Z. A. Majid. 2022. "General Overview on Cellulose and Cellulose Nanocrystals: Properties, Extraction, Application, and Sustainable Development." In *Environmental Management and Sustainable Development*, 93–114. Springer International Publishing. https://doi.org/10.1007/978-3-030-93932-8_7.
13. Calvino, C., N. Macke, R. Kato, and S. J. Rowan. 2020. "Development, Processing and Applications of Bio-Sourced Cellulose Nanocrystal Composites." *Progress in Polymer Science* 103: 101221. https://doi.org/10.1016/j.progpolymsci.2020.101221.
14. Okwuwa, C. C., F. Adam, F. Mohd Said, and M. E. Ries. 2023. "Cellulose Dissolution for Edible Biocomposites in Deep Eutectic Solvents: A Review." *Journal of Cleaner Production* 427: 139166. https://doi.org/10.1016/j.jclepro.2023.139166.
15. Parthasarathi, R., G. Bellesia, S. P. S. Chundawat, B. E. Dale, P. Langan, and S. Gnanakaran. 2011. "Insights Into Hydrogen Bonding and Stacking Interactions in Cellulose." *The Journal of Physical Chemistry A* 115(49): 14191–202. https://doi.org/10.1021/jp203620x.
16. Babaei-Ghazvini, A., B. Vafakish, R. Patel, K. J. Falua, M. J. Dunlop, and B. Acharya. 2024. "Cellulose Nanocrystals in the Development of Biodegradable Materials: A Review on CNC Resources, Modification, and Their Hybridization." *International Journal of Biological Macromolecules* 258: 128834. https://doi.org/10.1016/j.ijbiomac.2023.128834.
17. Santana-Mayor, Á., R. Rodríguez-Ramos, A. V. Herrera-Herrera, B. Socas-Rodríguez, and M. Á. Rodríguez-Delgado. 2021. "Deep Eutectic Solvents. the New Generation of Green Solvents in Analytical Chemistry." *TrAC, Trends in Analytical Chemistry* 134: 116108. https://doi.org/10.1016/j.trac.2020.116108.
18. Prabhune, A., and R. Dey. 2023. "Green and Sustainable Solvents of the Future: Deep Eutectic Solvents." *Journal of Molecular Liquids* 379: 121676. https://doi.org/10.1016/j.molliq.2023.121676.
19. Wei, L., W. Zhang, J. Yang, Y. Pan, H. Chen, and Z. Zhang. 2023. "The Application of Deep Eutectic Solvents Systems Based on Choline Chloride in the Preparation of Biodegradable Food Packaging Films." *Trends in Food Science & Technology* 139: 104124. https://doi.org/10.1016/j.tifs.2023.104124.
20. Alcalde, R., M. Atilhan, and S. Aparicio. 2018. "On the Properties of (Choline Chloride + Lactic Acid) Deep Eutectic Solvent With Methanol Mixtures." *Journal of Molecular Liquids* 272: 815–20. https://doi.org/10.1016/j.molliq.2018.10.052.
21. Ramli, N. A., F. Adam, M. E. Ries, and S. F. Ibrahim. 2024. "DES-Ultrasonication Treatment of Cellulose Nanocrystals and the Reinforcement in Carrageenan Biocomposite." *International Journal of*

Biological Macromolecules 270: 132385. https://doi.org/10.1016/j.ijbiomac.2024.132385.

22. Ramli, N. A., F. Rosli, M. Aiman Hamdan, and F. Adam. 2024. "Synthesis of Carrageenan-Based Biocomposite Plasticized With Deep Eutectic Solvent and Characterization of Its Mechanical Properties (Sintesis Biokomposit Berasaskan Karaginan Diplastikkan Dengan Pelarut Eutektik Dalam Dan Penyifatan Ciri-Ciri Mekanikal)." *Malaysian Journal of Analytical Sciences* 28.
23. Zhang, C., Z. Zhou, M. Xi, H. Ma, J. Qin, and H. Jia. 2024. "Molecular Modeling to Elucidate the Dynamic Interaction Process and Aggregation Mechanism Between Natural Organic Matters and Nanoplastics." *Eco-Environment & Health* 4(1): 100122. https://doi.org/10.1016/j.eehl.2024.08.004.
24. Ramli, N. A., F. Adam, K. N. Mohd Amin, A. M. Nor, and M. E. Ries. 2023. "Evaluation of Mechanical and Thermal Properties of Carrageenan/Hydroxypropyl Methyl Cellulose Hard Capsule." *Canadian Journal of Chemical Engineering* 101(3): 1219–34. https://doi.org/10.1002/cjce.24595.
25. Xu, H., W. Pan, R. Wang, D. Zhang, and C. Liu. 2012. "Understanding the Mechanism of Cellulose Dissolution in 1-Butyl-3-Methylimidazolium Chloride Ionic Liquid via Quantum Chemistry Calculations and Molecular Dynamics Simulations." *Journal of Computer-Aided Molecular Design* 26(3): 329–37. https://doi.org/10.1007/s10822-012-9559-9.
26. Wang, L., A. Azizi, T. Xu, S. R. Kirk, and S. Jenkins. 2019. "Explanation of the Role of Hydrogen Bonding in the Structural Preferences of Small Molecule Conformers." *Chemical Physics Letters* 730: 206–12. https://doi.org/10.1016/j.cplett.2019.06.015.
27. Bangar, S. P., and W. S. Whiteside. 2021. "Nano-Cellulose Reinforced Starch Bio Composite Films – A Review on Green Composites." *International Journal of Biological Macromolecules* 185: 849–60. https://doi.org/10.1016/j.ijbiomac.2021.07.017.
28. Oliaei, E., P. Olsén, T. Lindström, and L. A. Berglund. 2022. "Highly Reinforced and Degradable Lignocellulose Biocomposites by Polymerization of New Polyester Oligomers." *Nature Communications* 13(1): 5666. https://doi.org/10.1038/s41467-022-33283-z.
29. Zhang, H., J. Lang, P. Lan, H. Yang, J. Lu, and Z. Wang. 2020. "Study on the Dissolution Mechanism of Cellulose by ChCl-Based Deep Eutectic Solvents." *Materials* 13(2): 278. https://doi.org/10.3390/ma13020278.
30. Jha, M. K., A. Malik, and H. K. Kashyap. 2023. "How Hydrogen Bond Donor Acceptor Ratio and Water Content Impact Heterogeneity in Microstructure and Dynamics of N,N-Diisooctylacetamide and Decanol Based Hydrophobic Deep Eutectic Solvent." *Journal of Molecular Liquids* 385: 122127. https://doi.org/10.1016/j.molliq.2023.122127.
31. Li, C., C. Huang, Y. Zhao, C. Zheng, H. Su, L. Zhang, W. Luo, H. Zhao, S. Wang, and L.-J. Huang. 2021. "Effect of Choline-Based Deep Eutectic Solvent Pretreatment on the Structure of Cellulose and Lignin in Bagasse." *Processes* 9(2): 384. https://doi.org/10.3390/pr9020384.
32. Kalmer, R. R., M. M. Haddadan, M. Azizi, M. Ghanbari, D. Samandarian, A. Sadjadinia, H. Ramezanalizadeh, A. Karimi, and M. Golizadeh. 2023. "Industrial Manufacture of Enteric Hard Capsules Using Novel Formulations Based on Hypromellose Phthalate/Gelatin and Investigation of Pantoprazole Release." *ACS Omega* 8(12): 11293–303. https://doi.org/10.1021/acsomega.2c08290.
33. Bakó, I., S. Pothoczki, and L. Pusztai. 2023. "Connecting Diffraction Experiments and Network Analysis Tools for the Study of Hydrogen-Bonded Networks." *Journal of Physical Chemistry B* 127(14): 3109–18. https://doi.org/10.1021/acs.jpcb.2c07740.
34. Kebiroglu, H., and F. Ak. 2023. "Molecular Structure, Geometry Properties, HOMO-LUMO, and MEP Analysis of Acrylic Acid Based on DFT Calculations." *Journal of Physical Chemistry and Functional Materials* 6(2): 92–100. https://doi.org/10.54565/jphcfum.1343235.
35. Ramli, N. A., F. Adam, K. N. Mohd Amin, N. F. Abu Bakar, and M. E. Ries. 2022. "Mechanical and Thermal Evaluation of Carrageenan/Hydroxypropyl Methyl Cellulose Biocomposite Incorporated With Modified Starch Corroborated by Molecular Interaction Recognition." *ACS Applied Polymer Materials* 5(1): 182–92. https://doi.org/10.1021/acsapm.2c01426.
36. Ai, W.-T., W.-K. Su, and F. Su. 2023. "Solvents Influence 1H NMR Chemical Shifts and Complete 1H and 13C NMR Spectral Assignments for Florfenicol." *Pharmaceutical Fronts* 5(4): e288–96. https://doi.org/10.1055/s-0043-1777285.
37. Qiao, H., L. Li, J. Wu, Y. Zhang, Y. Liao, H. Zhou, and D. Li. 2020. "High-Strength Cellulose Films Obtained by the Combined Action of Shear Force and Surface Selective Dissolution." *Carbohydrate Polymers* 233: 115883. https://doi.org/10.1016/j.carbpol.2020.115883.
38. Okwuwa, C. C., F. Adam, and M. E. Ries. 2025. "Nanocellulose Dissolution in Green Solvents: Enhancing Carrageenan Biocomposites for Sustainable Hard Capsule Production." *Cellulose* 32(9): 5335–59. https://doi.org/10.1007/s10570-025-06474-2.
39. Hamdan, M. A., M. A. Khairatun Najwa, R. Jose, D. Martin, and F. Adam. 2021. "Tuning Mechanical Properties of Seaweeds for Hard Capsules: A Step Forward for a Sustainable Drug Delivery Medium." *Food Hydrocolloids for Health* 1: 100023. https://doi.org/10.1016/j.fhfh.2021.100023.
40. Aiman Hamdan, M., F. Adam, and K. Najwa Mohd Amin. 2018. "Investigation of Mixing Time on Carrageenan-Cellulose Nanocrystals (CNC) Hard Capsule for Drug Delivery Carrier." *International Journal of Innovative Science and Research Technology* 3(1). www.ijisrt.com457.
41. Aiman Hamdan, M., N. Hikmah Sulaiman, K. Najwa Mohd Amin, and F. Adam. 2021. "Moisture Content and Mechanical Properties Reduction of Hard Capsules upon Prolong Drying Process." *IOP Conference Series: Materials Science and Engineering* 1092(1): 012057. https://doi.org/10.1088/1757-899X/1092/1/012057.
42. Maryam Adilah, Z. A., F. Han Lyn, B. Nabilah, B. Jamilah, C. Gun Hean, and Z. A. Nur Hanani. 2022. "Enhancing the Physicochemical and Functional Properties of Gelatin/Graphene Oxide/Cinnamon Bark Oil Nanocomposite Packaging Films Using Ferulic Acid." *Food Packaging and Shelf Life* 34: 100960. https://doi.org/10.1016/j.fpsl.2022.100960.
43. Cao, B., J. Du, D. Du, H. Sun, X. Zhu, and H. Fu. 2016. "Cellobiose as a Model System to Reveal Cellulose Dissolution Mechanism in Acetate-Based Ionic Liquids: Density Functional Theory Study Substantiated by NMR Spectra." *Carbohydrate Polymers* 149: 348–56. https://doi.org/10.1016/j.carbpol.2016.04.128.
44. Xu, H., W. Pan, R. Wang, D. Zhang, and C. Liu. 2012. "Understanding the Mechanism of Cellulose Dissolution in 1-Butyl-3-Methylimidazolium Chloride Ionic Liquid via Quantum Chemistry Calculations and Molecular Dynamics Simulations." *Journal of Computer-Aided Molecular Design* 26(3): 329–37. https://doi.org/10.1007/s10822-012-9559-9.
45. Tong, Z., S. Zeng, X. Li, W. Wang, Q. Xia, and H. Yu. 2023. "Glycosidic Bond Protection of Cellulose During Solvent Dissolution by Coordination Interaction Competition Strategy." *Carbohydrate Polymers* 328: 121665. https://doi.org/10.1016/j.carbpol.2023.121665.
46. Abdul Mudalip, S. K., M. R. Abu Bakar, P. Jamal, and F. Adam. 2019. "Prediction of Mefenamic Acid Solubility and Molecular Interaction Energies in Different Classes of Organic Solvents and Water." *Industrial & Engineering Chemistry Research* 58(2): 762–70. https://doi.org/10.1021/acs.iecr.8b02722.
47. Penner, P., and A. Vulpetti. 2024. "QM Assisted ML for 19F NMR Chemical Shift Prediction." *Journal of Computer-Aided Molecular Design* 38(1): 4. https://doi.org/10.1007/s10822-023-00542-0.
48. Speciale, I., A. Notaro, P. Garcia-Vello, F. Di Lorenzo, S. Armiento, A. Molinaro, R. Marchetti, A. Silipo, and C. De Castro. 2022. "Liquid-State NMR Spectroscopy for Complex Carbohydrate Structural

Analysis: A Hitchhiker's Guide." *Carbohydrate Polymers* 277: 118885. https://doi.org/10.1016/j.carbpol.2021.118885.

49. Gundupalli, M. P., K. Cheenkachorn, S. Chuetor, S. Kirdponpattara, S. P. Gundupalli, P. L. Show, and M. Sriariyanun. 2023. "Assessment of Pure, Mixed and Diluted Deep Eutectic Solvents on Napier Grass (*Cenchrus purpureus*): Compositional and Characterization Studies of Cellulose, Hemicellulose and Lignin." *Carbohydrate Polymers* 306: 120599. https://doi.org/10.1016/j.carbpol.2023.120599.
50. Nandiyanto, A. B. D., R. Oktiani, and R. Ragadhita. 2019. "How to Read and Interpret FTIR Spectroscope of Organic Material." *Indonesian Journal of Science and Technology* 4(1): 97–118. https://doi.org/10.17509/ijost.v4i1.15806.
51. Liu, Q., H. Yu, T. Mu, Z. Xue, and F. Xu. 2021. "Robust Superbase-Based Emerging Solvents for Highly Efficient Dissolution of Cellulose." *Carbohydrate Polymers* 272: 118454. https://doi.org/10.1016/j.carbpol.2021.118454.
52. Ci, Y., Y. Ma, T. Chen, F. Li, and Y. Tang. 2024. "Facile Dissolution of Cellulose by Superbase-Derived Ionic Liquid Using Organic Solvents as Co-Solvents at Mild Temperatures." *Carbohydrate Polymers* 330: 121836. https://doi.org/10.1016/j.carbpol.2024.121836.
53. Kachangoon, R., J. Vichapong, Y. Santaladchaiyakit, R. Burakham, and S. Srijaranai. 2020. "An Eco-Friendly Hydrophobic Deep Eutectic Solvent-Based Dispersive Liquid-Liquid Microextraction for the Determination of Neonicotinoid Insecticide Residues in Water, Soil and Egg Yolk Samples." *Molecules* 25(12): 2785. https://doi.org/10.3390/molecules25122785.
54. Liu, Z., Y. Hou, S. Hu, and Y. Li. 2020. "Possible Dissolution Mechanism of Alkali Lignin in Lactic Acid-Choline Chloride Under Mild Conditions." *RSC Advances* 10(67): 40649–57. https://doi.org/10.1039/d0ra07808e.
55. Feng, Y., G. Liu, H. Sun, C. Xu, B. Wu, C. Huang, and B. Lei. 2022. "A Novel Strategy to Intensify the Dissolution of Cellulose in Deep Eutectic Solvents by Partial Chemical Bonding." *Bioresources* 17(3): 4167–85. https://doi.org/10.15376/biores.17.3.4167-4185.
56. Khater, E.-S., A. Bahnasawy, B. A. Gabal, W. Abbas, and O. Morsy. 2023. "Effect of Adding Nano-Materials on the Properties of Hydroxypropyl Methylcellulose (HPMC) Edible Films." *Scientific Reports* 13(1): 5063. https://doi.org/10.1038/s41598-023-32218-y.
57. Sanyang, M. L., S. M. Sapuan, M. Jawaid, M. R. Ishak, and J. Sahari. 2016. "Recent Developments in Sugar Palm (*Arenga pinnata*) Based Biocomposites and Their Potential Industrial Applications: A Review." *Renewable and Sustainable Energy Reviews* 54: 533–49. https://doi.org/10.1016/j.rser.2015.10.037.
58. Cazón, P., E. Morales-Sanchez, G. Velazquez, and M. Vázquez. 2022. "Measurement of the Water Vapor Permeability of Chitosan Films: A Laboratory Experiment on Food Packaging Materials." *Journal of Chemical Education* 99(6): 2403–8. https://doi.org/10.1021/acs.jchemed.2c00449.
59. Wan Ishak, W. H., N. A. Rosli, and I. Ahmad. 2020. "Influence of Amorphous Cellulose on Mechanical, Thermal, and Hydrolytic Degradation of Poly(Lactic Acid) Biocomposites." *Scientific Reports* 10(1): 11342. https://doi.org/10.1038/s41598-020-68274-x.
60. Gygli, G., X. Xu, and J. Pleiss. 2020. "Meta-Analysis of Viscosity of Aqueous Deep Eutectic Solvents and Their Components." *Scientific Reports* 10(1): 21395. https://doi.org/10.1038/s41598-020-78101-y.
61. Hou, Y., B. Zhang, M. Gao, S. Ren, and W. Wu. 2023. "Densities, Viscosities and Specific Heat Capacities of Deep Eutectic Solvents Composed of Ethanediol + Betaine and Ethanediol + L-Carnitine for Absorbing SO_2." *The Journal of Chemical Thermodynamics* 179: 106999. https://doi.org/10.1016/j.jct.2022.106999.